



Co-published by
Institute of Fluid-Flow Machinery
Polish Academy of Sciences
Committee on Thermodynamics and Combustion
Polish Academy of Sciences

Copyright©2024 by the Authors under licence CC BY-NC-ND 4.0

<http://www.imp.gda.pl/archives-of-thermodynamics/>



A comparative numerical evaluation of solar air heater performance having W-contoured, taper-contoured and reverse taper-contoured turbulators

Abhishek Ghildyal^a, Vijay Singh Bisht^a, Prabhakar Bhandari^b, Subham Thapliyal^c, Shivasheesh Kaushik^{d*}, Lalit Ranakoti^e, Raghubeer Singh Bangari^f, Ayushman Srivastav^g, Nikhil Kanojia^g, Ashwarya Raj Paul^h

^aDepartment of Mechanical Engineering, Veer Madho Singh Bhandari Uttarakhand Technical University, Dehradun 248007, India

^bDepartment of Mechanical Engineering, School of Engineering and Technology, K.R. Mangalam University, Gurugram, Haryana 122103, India

^cDepartment of Mechanical Engineering, Uttaranchal University, Dehradun, India

^dDepartment of Mechanical Engineering, Shivalik College of Engineering Dehradun, India

^eDepartment of Mechanical Engineering, Graphic Era Deemed to Be University, Dehradun 248002, Uttarakhand, India

^fDepartment of Mechanical Engineering, Graphic Era Hill University, Dehradun 248002, Uttarakhand, India

^gDepartment of Mechanical Engineering, U.P.E.S., Dehradun, India

^hDepartment of Mechanical Engineering, Vellore Institute of Technology, Vellore, India

*Corresponding author email: shivasheeshkecu@gmail.com

Received: 01.02.2024; revised: 17.09.2024; accepted: 29.10.2024

Abstract

The use of different turbulators in solar air heaters can significantly impact their thermal and hydraulic performance. This study compares solar air heaters equipped with W-contoured, taper-contoured, and reverse taper-contoured turbulators. It examines heat transfer coefficients, pressure drops, velocity contours, turbulent kinetic energy contours, and thermal performance factors for these systems under varying operating conditions. The air Reynolds number ranges from 4000 to 18 000, while design parameters such as relative roughness height and relative pitch ratio remain constant for accurate comparison. The simulations were conducted with a uniform heat flux of 1200 W/m². The W-shaped contour roughness achieved the greatest heat transfer coefficient, surpassing both the tapered and reverse tapered configurations. In terms of friction factor, the tapered contour on the absorber plate led, followed by the reverse tapered and W-shaped contours. Overall, the W-shaped contour delivered the best performance. At lower Reynolds numbers, the reverse tapered contour outperformed the tapered contour, whereas at higher Reynolds numbers, the tapered contour showed superior performance compared to the reverse tapered contour.

Keywords: W-contoured; Taper-contoured; Reverse taper-contoured; Turbulent kinetic energy; Thermo-hydraulic performance

Vol. 45(2024), No. 4, 189–196; doi: 10.24425/ather.2024.152008

Cite this manuscript as: Ghildyal, A., Bisht, V.S., Bhandari, P., Thapliyal, S., Kaushik, S., Ranakoti, L., Bangari, R.S., Srivastav, A., Kanojia, N., & Paul, A.R. (2024). A comparative numerical evaluation of solar air heater performance having W-contoured, taper-contoured and reverse taper-contoured turbulators. *Archives of Thermodynamics*, 45(4), 189–196.

1. Introduction

Commercial energy sources have played a role in fostering economic development, but they have also had a harmful impact on

the environment and society's health due to the greenhouse effect and global warming. In contrast, renewable energy sources offer a solution to meet global energy demands while safeguarding our surroundings. Additionally, sustainable energy systems,

Nomenclature

C_p – specific heat, J/(kg K)
 D_h – hydraulic diameter, mm
 e – roughness height, mm
 f – friction factor
 h – heat transfer coefficient, W/(m² K)
 k – thermal conductivity, W/(m K)
 L – length, mm
 Nu – average Nusselt number
 δp – pressure drop, Pa
 P – roughness pitch, mm
 Re – Reynolds number
 T – temperature, K
 u, v – velocity components, m/s

x, y – Cartesian coordinates, m

Greek symbols

α – thermal diffusivity, m²/s
 ν – kinematic viscosity, m²/s
 ρ – fluid density, kg/m³

Subscripts and Superscripts

f – test section
 r – roughened
 s – smooth

Abbreviations and Acronyms

PEC – performance evaluation criterion
 SAH – solar air heater

often smaller and region-specific, address concerns related to electricity distribution, environmental impact, and capital costs. Unlike centralised plants based on commercial sources, sustainable equipment like wind turbines, solar panels, and biomass can be mass-produced cost-effectively and tailored to meet the energy needs of specific locations. Among all sustainable energy sources [1], solar power has gained significant prominence due to its abundance, cost-effectiveness, cleanliness, and noiseless operation, while also being environmentally friendly.

Various methods are present for collecting solar energy, the most common of which is the flat plate solar collector, which has a basic design and requires relatively less receiving. Flat plate collectors are used less frequently. Whereas, solar water heaters and solar air heaters (SAH) require regulating for all anticipated temperature ranges [2,3]. However, one significant challenge with SAHs is their suboptimal heat/thermal efficiency due to the slow heat transfer from the absorbing plate (AP) to the air in the duct. To address this issue, artificial turbulators like baffles and ribs are employed [4,5]. These create turbulence within the air duct, enhancing the heat transfer coefficient. However, they also lead to increased friction loss, so it is essential to place turbulators solely in the laminar subzone layer.

Various methods have been proposed by researchers to increase heat transfer through SAH like nanoparticles [6,7], phase change materials [8,9], microchannels [10–12], minichannels [13,14], active techniques [15], etc. It is observed that various design modifications in SAH were taken from other thermal devices like microchannels heat sinks [16,17], heat exchangers [18–20], spiral tube exchangers [21], heat pipes with inserts and baffles [22,23], electric vehicle battery cooling [24], electrical device cooling with fins [25], car radiator [26,27], etc. Some of the recent work covered in the area of SAH has been covered herein.

Khanlari et al. [28] study aimed to enhance the utilization time of a solar air collector by integrating a PCM (phase change material) unit and adding porous fins to shorten PCM melting time. The numerical analysis showed that adding the PCM unit extended the collector's utilization time, and increasing the number of porous fins significantly improved the system's performance and energy efficiency. Abdulmejeed et al. [29] examined

the performance of SAH with grooved absorber and triple-flow air channel modifications using numerical modelling and experimental evaluation. The combined SAH showed greater temperature differences than parallel-flow and triple-flow SAHs, with the parallel-flow SAH achieving thermal and exergy efficiencies of 59.51% and 29.09%, respectively, at a mass flow rate of 0.012 kg/s.

Tuncer et al. [30] study aimed to improve a solar drying system (SDS) by using a ZnO nano-enhanced absorber coating and an infrared heating system. The results showed that the combined use of these modifications significantly increased thermal and exergetic efficiencies and reduced drying time by 43.75% compared to the unmodified SDS.

Solar air heater performance can be enhanced using turbulators like Z-shaped baffles on the absorber plate as reported by Bohra et al. [31]. They found that for a blockage ratio of 0.3, with a relative pitch ratio of 1.5 and an attack angle of 45°, the maximum effective efficiency was achieved for Reynolds numbers between 5000 and 10 000. In another similar work, Semalty et al. [32] examined the effectiveness of a solar air heater with multiple ribs and an arc-shaped circular protrusion on the absorber plate, using Fluent simulations. The results indicated that the optimal thermal performance was achieved at a Reynolds number of 20 000, with specific roughness and protrusion parameters, improving thermal performance with minimal frictional pressure drop.

Singh et al. [33] performed a numerical investigation analysing the hydrothermal characteristics of SAH with S-shaped dimple roughness on the absorber plate, using Ansys Fluent for Reynolds numbers 4000 to 20 000. The study found that the optimal configuration, with a dimple diameter of 2.8 mm and relative roughness pitch of 10, yielded significantly higher Nusselt numbers and friction factors compared to smooth plates, achieving maximum thermo-hydraulic performance at a Reynolds number of 20 000. Haldia et al. [34] presented a numerical study comparing the effects of S-shaped and broken arc roughness on solar air heaters, finding that the optimal configuration for heat transfer is a gap of 0.9 mm and a pitch of 25 mm. This specific configuration significantly improves heat transfer but increases the friction factor, achieving the highest thermal performance

factor of 2.9 to 3.3, while a gap of 0.3 mm and the same pitch length shows the lowest performance.

Kumar et al. [35] explored the impact of S-shaped ribs and protrusions on the thermo-hydraulic performance of a SAH, examining various operating and design parameters. The optimal configuration, with a relative pitch roughness of 20, gap of 0.5 mm, and protrusion diameter of 0.3 mm, achieved the highest thermal performance factor of 2.5 to 3.1, while the least effective configuration had a pitch of 12 and protrusion diameter of 0.5 mm, resulting in a factor of 1.4 to 1.7. Kumar [36] experimentally analyses the heat transfer and friction factor of three-side artificially roughened solar air heaters with multiple-V and transverse wires compared to one-side roughened heaters. The three-side roughened heaters show a 24–76% increase in heat transfer rate and a 4–36% increase in friction factor, with air temperatures 34.6% higher than those in one-side roughened heaters, proving their superior performance both qualitatively and quantitatively. Ghritlahre [37] analyzes the energy and exergy performance of roughened solar air heaters with arc-shaped wire ribs using two flow arrangements: apex upstream and apex downstream. Results show that the apex upstream flow configuration achieves a maximum thermal efficiency of 73.2% and exergy efficiency of 2.64% at a mass flow rate of 0.022 kg/s, while the apex downstream flow configuration reaches a thermal efficiency of 69.4% and exergy efficiency of 1.89% under the same conditions.

Patel and Lanjewar [38] use exergy analysis to evaluate the performance of a solar air heater with a W-shaped roughened absorber surface, comparing it to a smooth plate under identical conditions. The analysis shows that the W-shaped roughened surface improves exergetic efficiency by up to 51% with a relative roughness height of 0.03375 and a rib angle of 60° , helping to optimize the design parameters for better performance. Chaudhari et al. [39] focus on optimizing the exergetic efficiency of a solar air heater with inverted L-shaped ribs by improving heat transfer rates. The analysis, conducted at a constant heat flux of 1000 W/m^2 , determined that a relative roughness pitch of 17.86 within Reynolds numbers of 3000 to 18 000 yields optimal exergy performance, with temperature rises between 0.005 and 0.04. Ghildyal et al. [40] considered D-shaped, Reverse D-shaped and U-shaped turbulators in SAH and observed that the U-shaped turbulator achieved the best overall performance.

The present research work focuses on investigating the effects of W-contoured, taper-contoured, and reverse taper-contoured turbulators in solar air heaters, as depicted in Fig.1. The novelty of this research lies in its comparative numerical evaluation of solar air heater performance using three distinct turbulators geometries. This study is pioneering in its approach to geometric diversity, numerical simulation, comprehensive comparison and practical implications. Employing advanced numerical methods to simulate and evaluate the performance of these geometries, provides detailed insights into their thermal and hydraulic characteristics. Offering a direct comparison of the performance enhancements and efficiency gains of each turbulator type helps to identify the most effective design for solar air heaters.

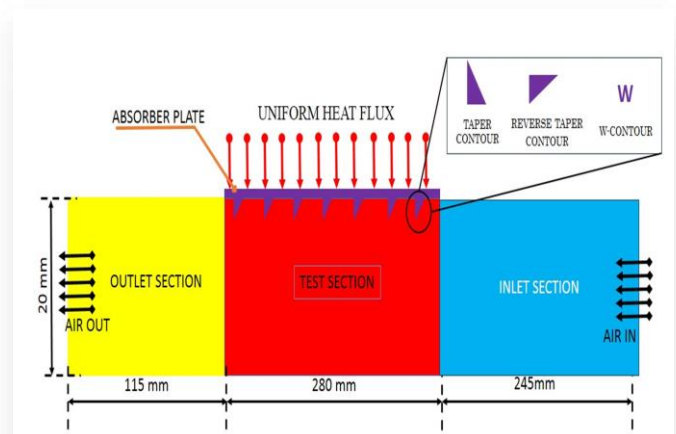


Fig. 1. Schematic diagram of solar air heaters with dimensions and different contours used for roughness.

The primary objective of this research is to enhance the performance of solar air heaters by evaluating and comparing the effectiveness of W-contoured, taper-contoured, and reverse taper-contoured turbulators. This is done by determining the impact of each turbulator design on heat transfer rates, pressure drop, and overall thermal efficiency. Further, the study also highlights potential areas for future research exploration of additional turbulator geometries or configurations.

2. Details of computational domain and grid generation

A two-dimensional computational fluid dynamics study was performed to determine how the performance of SAH changes when a roughened absorber plate is utilized. In the present research work, W-contour, taper-shaped contour, and reverse taper-contoured turbulators were used. The computational domain has 3 regions and is rectangular, measuring 20 mm in height and 640 mm in length: the entry length ($L_1 = 245 \text{ mm}$), the test region ($L_2 = 280 \text{ mm}$), and the exit length ($L_3 = 115 \text{ mm}$). Under the absorber plate, turbulators are mounted. In the current study, constant relative roughness height ($e/D_h = 0.021$) and pitch ratio ($P/e = 14.285$) are used for all three turbulators. The choice of particular dimensions was based on previous literature. The air temperature at the inflow is considered to be 300 K.

Solar air heater modelling is done in Ansys Design Modular during the pre-processing phase of this investigation. The Ansys ICEM platform is used for computational domain meshing. The simulations were conducted using Ansys Fluent, a commercial software based on the finite volume method. The momentum and energy equations were discretized using a second-order upwind scheme. The pressure-velocity coupling was addressed using the SIMPLE (semi-implicit method for pressure-linked equations) algorithm. To solve the resulting system of algebraic equations, the Gauss-Seidel iterative method was employed. This numerical approach has been widely used by various researchers for similar problems [41,42].

A homogeneous structural quadrilateral mesh with $y^+ = 1$ (nondimensional distance from the wall) is used to build the computational domain. To accomplish uniform blending throughout the sector, featured face mesh has been adapted with a 0.2 mm body size. Figure 2 depicts the uniform structural mesh of SAH with W-contoured turbulators. To perform the grid independence test, the smooth SAH was simulated for a number of grid cells ranging from 115 200 to 480 000 for a Reynolds number of 12 000. The complete details of the test are tabulated in Table 1. It was observed that a mesh of 320 000 cells has provided optimum results in lesser computational time. So, the same grid cells were opted for all simulations.

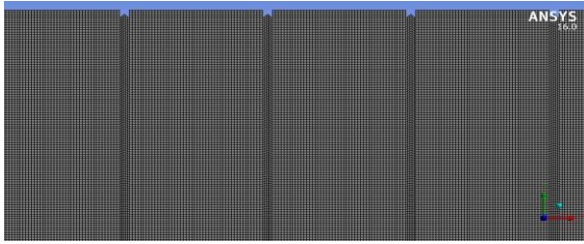


Fig. 2. Face integration of SAH with W-contoured turbulators.

Table 1. Grid independence test performed on smooth SAH.

No.	Number of grid cells	Nusselt number
1	115 200	44.00
2	192 000	39.0
3	320 000	36.44
4	480 000	36.1

2.1. Governing equations

The governing equations for the numerical model of a solar air heater are as follows:

- The continuity equation for two-dimensional steady fluid flow, which represents the conservation of mass for a fluid under motion:

$$\frac{\partial u}{\partial x} + \frac{\partial v}{\partial y} = 0, \tag{1}$$

where u and v are the velocity vector components in x and y directional coordinates, respectively.

- The momentum equations for the X and Y directions are given by:

X-momentum equation:

$$u \frac{\partial u}{\partial x} + v \frac{\partial u}{\partial y} = \frac{1}{\rho} \frac{\partial p}{\partial x} + \nu \left(\frac{\partial^2 u}{\partial x^2} + \frac{\partial^2 u}{\partial y^2} \right), \tag{2}$$

Y-momentum equation:

$$u \frac{\partial v}{\partial x} + v \frac{\partial v}{\partial y} = \frac{1}{\rho} \frac{\partial p}{\partial y} + \nu \left(\frac{\partial^2 v}{\partial x^2} + \frac{\partial^2 v}{\partial y^2} \right), \tag{3}$$

where ρ is the fluid density, p is the pressure and ν is the kinematic viscosity.

- For steady and incompressible flow with constant thermal conductivity, no compression work and no heat generation, the energy equation is given by:

$$u \frac{\partial T}{\partial x} + v \frac{\partial T}{\partial y} = \alpha \left(\frac{\partial^2 T}{\partial x^2} + \frac{\partial^2 T}{\partial y^2} \right), \tag{4}$$

where T represents temperature and α is the thermal diffusivity.

The mean Nusselt number is defined as:

$$Nu_r = \frac{h D_h}{k}, \tag{5}$$

where h , D_h and k stand for the coefficient of heat transfer, hydraulic diameter and thermal conductivity, respectively.

The factor of friction (f) is defined as:

$$f = \frac{2(\delta p) D_h}{4 \rho L_f V^2}, \tag{6}$$

where δp represents the pressure difference, L_f is the length and V is the velocity.

Performance evaluation criterion is defined as

$$PEC = \frac{h_r}{h_s} \left(\frac{\delta p_r}{\delta p_s} \right)^{\frac{1}{3}}, \tag{7}$$

where h and δp stand for the heat transfer coefficient and pressure drop, respectively, and subscripts r and s refer to roughened and smooth SAHs, respectively.

2.2. Confirmation of findings

The numerical model for the smooth solar air heater was validated by comparing the average Nusselt number and the friction factor with the well-known equations, as depicted in Fig.3. The average Nusselt number from the model was compared with the Dittus-Boelter equation, and the results showed a slight variation of 2–4% between them. Additionally, the friction factor was compared with the Blasius friction equation, and the results were found to be in good agreement, validating the numerical model. The Dittus-Boelter equation and the Blasius equation for smooth solar air heater are as follows:

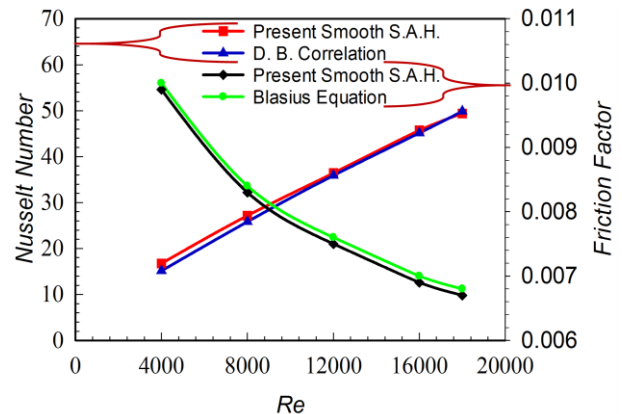


Fig. 3. Validation plot of smooth SAH with established correlation.

$$Nu_s = 0.023Re_s^{0.8}Pr_s^{0.4}, \quad (8)$$

$$f_s = 0.0791Re_s^{-0.25}. \quad (9)$$

3. Results and discussion

The variation of heat transfer coefficient with Reynolds number (Re) for different configuration of SAH is depicted in Fig. 4. The utilization of a textured surface on the solar air heater duct demonstrated a noteworthy improvement in the heat transfer rate compared to a smooth surface solar air heater. Nevertheless, the enhancement in heat transfer is minimal at low Reynolds numbers and escalates as the Reynolds number increases. Two main observations can be deduced from Fig. 4. Firstly, as the Reynolds number rises, there is a concurrent increase in the heat transfer coefficient for all solar air heater configurations. The rate of this increase in the heat transfer coefficient is higher for the roughened configuration compared to the smooth solar air heater case. Secondly, regardless of the variation in surface roughness, it was noted that the trend of heat transfer coefficient with Reynolds number remains consistent for all cases. Moreover, the W-shaped contour roughness exhibited the highest heat transfer coefficient value, followed by the tapered contour and reverse tapered contour configurations.

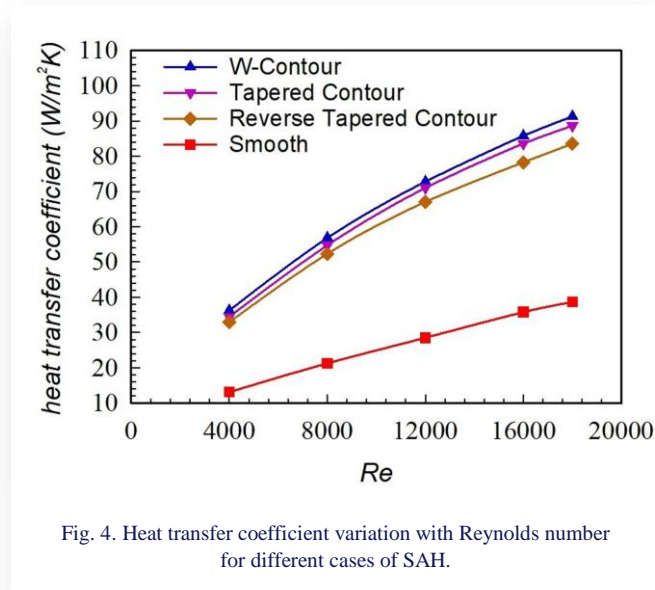


Fig. 4. Heat transfer coefficient variation with Reynolds number for different cases of SAH.

Just like the examination of heat transfer, an analysis of fluid flow was conducted by considering the pressure drop for various solar air heater configurations. It is recognized that incorporating vortex generators or turbulators on the solar air heater impacts the fluid flow parameter, specifically the pressure drop. Figure 5 demonstrates the variation of pressure drop in the SAH with Re for different configurations. It is obvious that the pressure drop in SAH with turbulators is greater than in the smooth SAH, due to obstruction in the flow field and disturbance of laminar sublayer.

Consequently, SAH with tapered contour roughness on the absorber plate yields a higher friction factor, followed by reverse tapered and W-shaped contour roughness. Both reverse tapered and W-shaped contour roughness SAHs show very marginal dif-

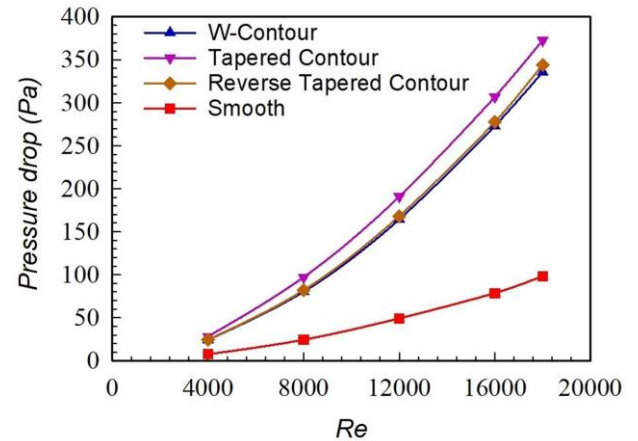


Fig. 5. Pressure drop variation with Reynolds number for different cases of SAH.

ference in pressure drop while tapered contour SAH demonstrates less difference at low Re value and the difference with other roughened SAH keeps on increasing with Re value.

Figure 6 shows the contours of velocity for each of the three coarsenesses in SAH. Once the flow is stabilized, contours of velocity reveal the creation of an eddy near the rib. A separation occurs as a result of the abrupt expansion of fluid downstream of the rib. This causes a rise in flow velocity at the upper surface of the rib, which generates turbulence. As a result, vortices form on the upper surface of the rib.

The turbulator/ribs prevent the creation of the boundary layer. As a result, the turbulent kinetic energy increases. Figure 7 displays the contours of turbulence kinetic energy for each of the three coarsenesses. The W-contour has a succession of comparable and recurring turbulence kinetic energy profiles, which simply illustrate the intensification of instability in turbulator, which increases the rate of the transfer of heat. W-contour turbulators outperform the other two types of turbulators in terms of heat transfer augmentation.

Figure 8 depicts variation of performance evaluation criterion (PEC) with Re for roughened SAH, considering smooth SAH as a reference model. As all roughened SAHs showed values above 1, this denotes that SAH with turbulators has better overall performance.

Further, it was observed that PEC keeps on decreasing with Re value for all cases. Among all the cases, W-contour has shown highest performance. While at low Re value, reverse tapered contour is better than tapered contour and at higher Re value, tapered contour is better than reverse tapered contour.

4. Conclusions

In present research work, a thorough 2D computational fluid dynamic analysis of a solar air heater with three types of turbulators are performed. The numerical analysis outcome can be summarized as follows:

- With the use of the k- ϵ turbulence model the verification and the computational domain are justified;

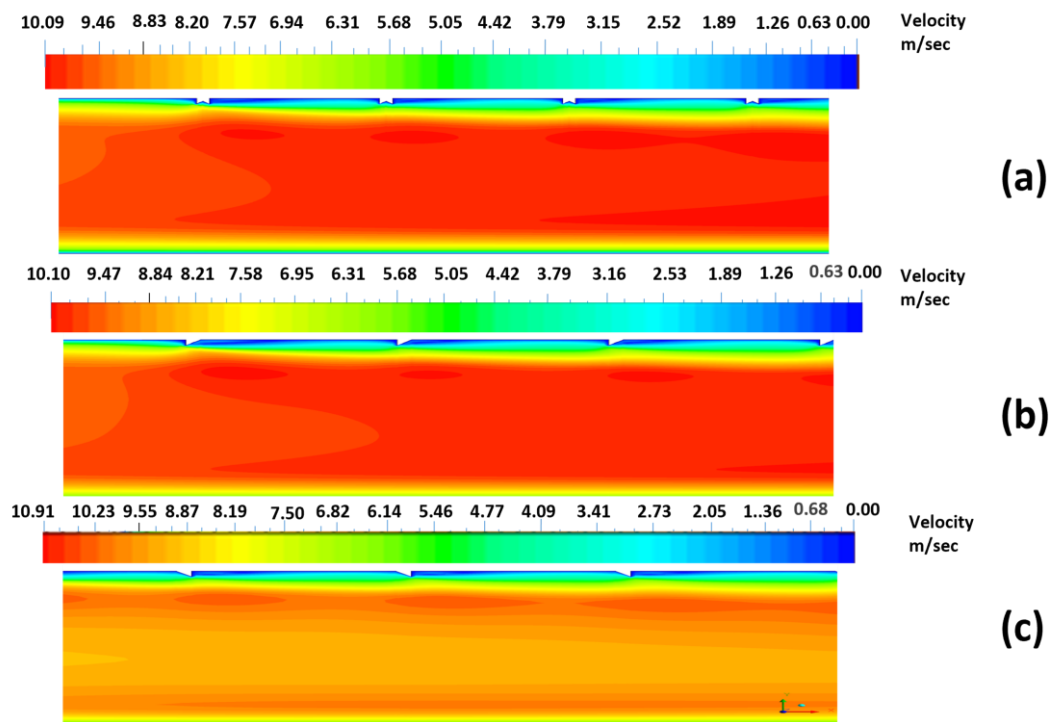


Fig. 6. Velocity contour for (a) W-contour, (b) reverse tapered contour, (c) tapered contour.

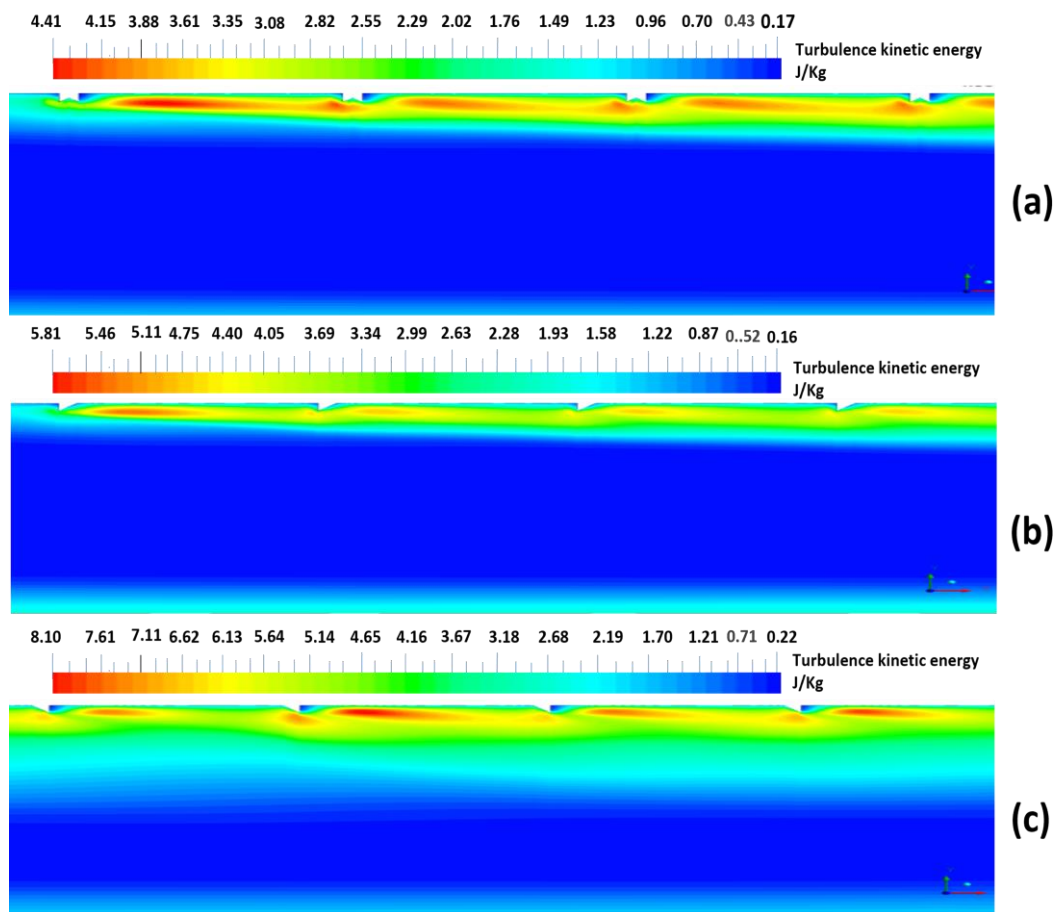


Fig. 7. Turbulence kinetic energy contour for (a) W-contour, (b) reverse tapered contour, (c) tapered contour.

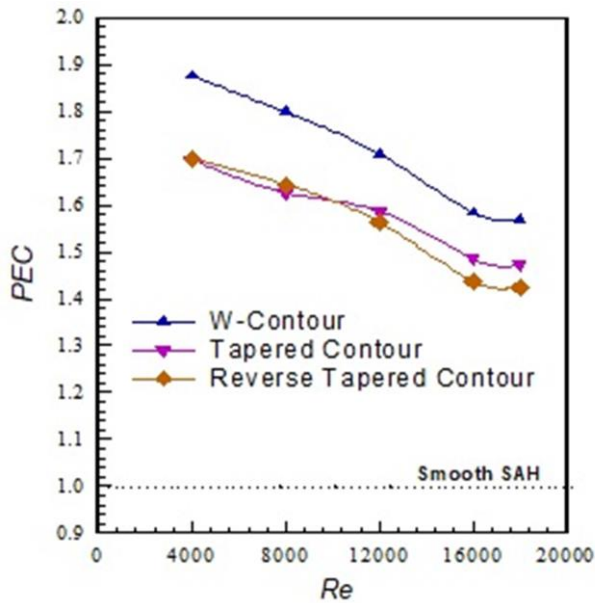


Fig. 8. Performance evaluation criteria variation with Re for roughened SAH.

- Among all configurations, SAH with W-contoured coarseness has the highest value of heat transfer coefficient, followed by taper-contoured and reverse taper-contoured configurations;
- In terms of hydraulic performance, SAH with taper-contoured roughness on the absorber plate yields a higher pressure drop, followed by reverse taper-contoured and W-shaped roughness configurations;
- Performance evaluation criterion, i.e. overall performance of the W-contour turbulator, is the highest irrespective of Reynolds number value.

As a result, a W-contoured turbulator might be explored for further experimental analysis and research on SAHs.

References

- [1] Bisht, V.S., Patil, A.K., & Gupta, A. (2018). Review and performance evaluation of roughened solar air heaters. *Renewable and Sustainable Energy Reviews*, 81(1), 954–977. doi: 10.1016/j.rser.2017.08.036
- [2] Bhandari, P., Varshney, L., & Bisht, V.S. (2018). Numerical analysis of hybrid solar water heating system using wire screen packed SAH. *1st International Conference on New Frontiers in Engineering, Science & Technology*, (pp. 415–442), 28-12 January, New Delhi, India.
- [3] Varshney, L., Bhandari, P., & Bisht, V.S. (2014). Performance evaluation of hybrid solar water heating system using wire screen packed solar air heater. *International Journal of Engineering Research and Applications (IJERA)*, 311–316. https://www.ijera.com/special_issue/ICETMEE/ME18%20rp5%20final.pdf
- [4] Kaushik, S., & Singh, S. (2019). Analysis on heat transmission and fluid flow attributes in solar air accumulator passage with diverse faux jaggedness silhouettes on absorber panel. *International Journal of Engineering and Advanced Technology*, 8(5S3), 32–41. doi: 10.35940/ijeat.E1011.0785S319
- [5] Kaushik, S., Panwar, K., & Vashisth, S. (2022). Investigating the thermionic effect of broken perforated curved ribs on solar pre-heater through CFD simulation. *Res Militaris* 12(5), 1508–1524.
- [6] Kumar, N., Singh, P., Redhewal, A.K., & Bhandari, P. (2015). A review on nanofluids applications for heat transfer in micro-channels. *Procedia Engineering*, 127, 1197–1202. doi: 10.1016/j.proeng.2015.11.461
- [7] Kaushik, S., Ali, S., Kanojia, N., Uniyal, V., Verma, A.K., Panwar, S., Uniyal, S., Goswami, S., Kindo, S., Som, D., & Yadav, N.K. (2023). Experimental and CFD analysis of fluid flow in a rectangular strip-based microchannel with nanofluid. *Materials Today: Proceedings*. doi: 10.1016/j.matpr.2023.05.647
- [8] Negi, A., Ranakoti, L., Bhandari, P., Khargotra, R., & Singh, T. (2024). Thermo-physical characteristics and storage material compatibility in nano-enhanced phase change materials for solar distillation applications: A critical assessment. *Solar Energy Materials and Solar Cells*, 271, 112870. doi: 10.1016/j.solmat.2024.112870
- [9] Uniyal, A., Prajapati, Y.K., Ranakoti, L., Bhandari, P., Singh, T., Gangil, B., Sharma, S., Upadhyay, V.V., & Eldin, S.M. (2022). Recent advancements in evacuated tube solar water heater: A critical review integration of phase change materials and nano-fluids with ETCs. *Energies*, 15(23), 8999. doi: 10.3390/en15238999
- [10] Bhandari, P., Prajapati Y.K., & Bisht, V.S. (2021). Heat transfer augmentation in micro pin fin heat sink using out of plane fluid mixing. *Proceedings of the 26th National and 4th International ISHMT-ASTFE Heat and Mass Transfer Conference*, (pp. 1595–1600), 17–20 December, Madras, India. doi: 10.1615/IHMTC-2021.2400
- [11] Bhandari, P., & Prajapati Y.K. (2020). Numerical analysis of different arrangement of square pin-fin microchannel heat sink. *Advances in Mechanical Engineering. Lecture Notes in Mechanical Engineering* (pp. 879–891). Springer, Singapore. doi: 10.1007/978-981-15-0124-1_79
- [12] Kaushik, S., Verma, A.K., Singh, S., Kanojia, N., Panwar, S., Uniyal, S., Goswami, S., Kindo, S., Som, D., & Yadav, N.K. (2023). Comparative analysis of fluid flow attributes in rectangular shape micro channel having external rectangular inserts with hybrid $Al_2O_3+ZNO+H_2O$ nano fluid and (H_2O) base fluid. *Evergreen – Joint Journal of Novel Carbon Resource Sciences & Green Asia Strategy*, 10(2), 851–862. doi: 10.5109/6792839
- [13] Kaushik, S., Uniyal, V., Ali, S., Kanojia, N., Verma, A.K., Joshi, S., Makhloga, M., Pargai, P.S., Sharma, S.K., Kumar, R., & Pal, S. (2023). Comparative analysis of fluid flow in mini channel with nano fluids and base fluid. *Materials Today: Proceedings*. doi: 10.1016/j.matpr.2023.05.363
- [14] Kaushik, S., Uniyal, V., Verma, A.K., Jha, A.K., Joshi, S., Makhloga, M., Pargai, P.S., Sharma, S.K., Kumar, R., & Pal, S. (2023). Comparative experimental and cfd analysis of fluid flow attributes in mini channel with hybrid $CuO+ZnO+H_2O$ nano fluid and (H_2O) base fluid. *Evergreen – Joint Journal of Novel Carbon Resource Sciences & Green Asia Strategy*, 10(1), 182–195. doi: 10.5109/6781069
- [15] Bhandari, P., Singh, J., Kumar K., & Ranakoti, L. (2022). A review on active techniques in microchannel heat sink for miniaturization problem in electronic industry: *Acta Innovations*, 45, 45–54. doi: 10.32933/ActaInnovations.45.4
- [16] Bhandari, P., Rawat, K.S., Prajapati, Y.K., Padalia, D., Ranakoti, L., & Singh, T. (2023). A review on design alteration in micro-channel heat sink for augmented thermohydraulic performance. *Ain Shams Engineering Journal*, 15(2), 102417. doi: 10.1016/j.asej.2023.102417

- [17] Bhandari, P., Rawat, K., Prajapati, Y.K., Padalia, D., Ranakoti, L., & Singh, T. (2023). Design modifications in micro pin fin configuration of microchannel heat sink for single phase liquid flow: A review. *Journal of Energy Storage*, 66, 107548. doi: 10.1016/j.est.2023.107548
- [18] Kaushik, S., Singh, S., & Panwar, K. (2023). Experimental study of fluid flow properties in spiral tube heat exchanger with varying insert shape over spiral tube profile. *Materials Today Elsevier*, 80(1), 78–84. doi: 10.1016/j.matpr.2022.10.117
- [19] Kaushik, S., Singh, S., & Panwar, K. (2021). Comparative analysis of thermal and fluid flow behaviour of diverse nano fluid using Al₂O₃, ZnO, CuO nano materials in concentric spiral tube heat exchanger. *Materials Today: Proceedings*, 46(15), 6625–6630. doi: 10.1016/j.matpr.2021.04.1000
- [20] Singh, P., Bisht, V.S., & Bhandari, P. (2021). Numerical study of heat exchanger having protrusion and dimple roughened conical ring inserts. *Advances in Fluid and Thermal Engineering. Lecture Notes in Mechanical Engineering* (pp. 151–161). Springer, Singapore. doi: 10.1007/978-981-16-0159-0_14
- [21] Kaushik, S., Singh, S., Kanojia, N., Rawat, K., & Panwar, K. (2020). Comparative study for thermal and fluid flow peculiarities in cascading spiral inner tube heat exchanger with or without diverse inserts over spiral tube. *IOP Conference Series: Materials Science and Engineering*, 802, 012009. doi: 10.1088/1757-899X/802/1/012009
- [22] Kaushik, S., Mahar, V.S., Singh, S., Kshetri, R., Kumar, B., Mehta, J.S., Paul, A.R., Kumar, S., Vashisth, S., Pundir, R.S., & Kumar, A. (2024). Comparative experimental analysis of fluid flow in a concentric tube exchanger having semi hollow cylindrical macro inserts with nanofluid and base fluid. *Archives of Thermodynamics*, 45(2), 205–212. doi: 10.24425/ather.2024.150866
- [23] Uniyal, V., Joshi, S.K., Kaushik, S., & Kanojia, N. (2021). CFD investigation of transfer of the heat and turbulent flow in circular copper tube with perforated conical rings of aluminium material. *Materials Today: Proceeding*, 46(15), 6719–6725. doi: 10.1016/j.matpr.2021.04.217
- [24] Bisht, A.S., Bisht, V.S., Bhandari, P., Rawat, K.S., Alam, T., & Blecich, P. (2023). The use of a vortex generator for the efficient cooling of lithium-ion batteries in hybrid electric vehicles. *Processes*, 11(2), 500. doi: 10.3390/pr11020500
- [25] Kaushik, S., Singh, S., Kanojia, N., Naudiyal, R., Kshetri, R., Paul, A.R., Kumari, R., Kumar, A., & Kumar, S. (2021). Effect of introducing varying number of fins over LED light bulb on thermal behavior. *Materials Today: Proceeding*, 46(19), 9794–9799. doi: 10.1016/j.matpr.2020.10.876
- [26] Thapa, R.K., Bisht, V.S., Bhandari, P., & Rawat, K. (2022). Numerical study of car radiator using dimple roughness and nanofluid. *Archives of Thermodynamics*, 43(3), 125–140. doi: 10.24425/ather.2022.143175
- [27] Thapa, R.K., Bisht, V.S., Rawat, K., & Bhandari, P. (2023). Computational analysis of automobile radiator roughened with rib roughness. *Journal of Heat and Mass Transfer Research*, 9(2), 209–218. doi: 10.22075/jhmtr.2023.27617.1382
- [28] Khanlari, A., Aytac, I., Tuncer, A.D., Variyenli, H.I., & Şahin, H.N. (2014). Improving the performance of a PCM integrated solar air collector by adding porous fins over the bottom side of the absorber: A transient CFD study. *Journal of Energy Storage*, 90(A), 111847. doi: 10.1016/j.est.2024.111847
- [29] Abdulmejeed, A.E.A., Tuncer, A.D., Khanlari, A., & Gungor, A. (2024). Investigation of combined parallel and triple-pass v-corrugated solar air heater: A numerical and experimental study. *Process Safety and Environmental Protection*, 185, 1385–1398. doi: 10.1016/j.psep.2024.03.107
- [30] Tuncer, A.D., Amini, A., & Khanlari, A. (2023). Developing an infrared-assisted solar drying system using a vertical solar air heater with perforated baffles and nano-enhanced black paint. *Solar Energy*, 263, 111958. doi: 10.1016/j.solener.2023.111958
- [31] Bohra, J., Bisht, V.S., Bhandari, P., Rawat, K.S., Singh, J., Kumar, K., & Rawat, B. (2022). Effect of variable blockage height ratio on performance for solar air heater roughened with 45°-shaped baffles. *Materials Today: Proceedings*, 69(2), 153–157. doi: 10.1016/j.matpr.2022.08.279
- [32] Semalty, A., Bisht, V.S., Bhandari, P., Rawat, K.S., Singh, J., Kumar, K. & Dixit, A.K. (2022). Thermodynamic investigation on solar air heater having roughness as multiple broken arc and circular protrusion. *Materials Today: Proceedings*, 69(2), 181–186. doi: 10.1016/j.matpr.2022.08.336
- [33] Singh, J., Bisht, V.S., Bhandari, P., Kumar, K., Singh, J., Alam, T., Dixit, S., Singh, S., & Khusnutdinov, R. (2024). Computational parametric investigation of solar air heater with dimple roughness in S-shaped pattern. *International Journal on Interactive Design and Manufacturing*, 18, 2969–2979. doi: 10.1007/s12008-023-01392-8
- [34] Haldia, S., Bisht, V.S., Bhandari, P., Ranakoti, L., & Negi, A. (2024). Numerical assessment of solar air heater performance having broken arc and broken S-shaped ribs as roughness. *Archives of Thermodynamics*, 2024, 45(1), 23–31. doi: 10.24425/ather.2024.150435
- [35] Kumar, S., Bisht, V.S., Bhandari, P., Ranakoti, L., Negi, A., Bisht, A.S., & Padalia, D. (2024). Computational analysis of modified solar air heater having combination of ribs and protrusion in S-shaped configuration. *International Journal on Interactive Design and Manufacturing*. doi: 10.1007/s12008-024-01972-2
- [36] Kumar, D. (2023). Heat transfer and friction characteristics in three-side solar air heaters with the combination of multi-v and transverse wire roughness. *Archives of Thermodynamics*, 44(1), 63–87. doi: 10.24425/ather.2023.145877
- [37] Ghritlahre, H.K. (2021). An experimental study of solar air heater using arc shaped wire rib roughness based on energy and exergy analysis. *Archives of Thermodynamics*, 42(3), 115–139. doi: 10.24425/ather.2021.138112
- [38] Patel, S. S., & Lanjewar, A. (2019). Exergy based analysis of solar air heater duct with W-shaped rib roughness on the absorber plate. *Archives of Thermodynamics*, 40(4), 21–48. doi: 10.24425/ather.2019.130006
- [39] Chaudhari, M., Sharma, S.L., & Debbarma, A. (2023). Exergetic performance analysis of solar air heater with inverted L-shape ribs as roughness element. *Archives of Thermodynamics*, 44(3), 241–267. doi: 10.24425/ather.2023.147546
- [40] Ghildyal, A., Bisht, V.S., Rawat, K.S., & Bhandari, P. (2023). Effect of D-shaped, reverse D-shaped and U-shaped turbulators in solar air heater on thermo-hydraulic performance. *Archives of Thermodynamics*, 44(2), 3–20. doi: 10.24425/ather.2023.146556
- [41] Bhandari, P., Vyas, B., Padalia, D., Ranakoti, L., Prajapati, Y.K., & Bangri, R.S. (2024). Comparative thermo-hydraulic analysis of periodic stepped open micro pin-fin heat sink. *Archives of Thermodynamics*, 45(3), 99–105. doi: 10.24425/ather.2024.151228
- [42] Bhandari, P., & Prajapati, Y.K. (2021). Numerical study of fluid flow and heat transfer in stepped micro-pin-fin heat sink. *Fluid Mechanics and Fluid Power. Lecture Notes in Mechanical Engineering* (pp. 373–381). Springer, Singapore. doi: 10.1007/978-981-16-0698-4_40